Vibrationally Resolved Absorption and Emission Spectra of Rubrene Multichromophores: Temperature and Aggregation Effects

Fang Gao and Wan Zhen Liang*

Hefei National Laboratory for Physical Science at Microscale, and Department of Chemical Physics, University of Science and Technology of China, Hefei 230026, People's Republic of China

Yang Zhao*

School of Material Science and Engineering, Nanyang Technological University, Singapore 63978, Singapore

Received: May 3, 2009; Revised Manuscript Received: September 17, 2009

We present a theoretical study on the temperature-dependent absorption and photoluminescence spectroscopy of rubrene multichromophores by combining the time-dependent long-range-corrected density functional theory with the exciton model. The spectra of rubrene multichromophores up to heptamers are calculated, and the effects of exciton−phonon coupling and temperature on the photophysical properties of both *H*- and *J*-aggregated oligomers are addressed. It is found that the spectral behavior of rubrene aggregates is very much dependent on aggregation details. As the temperature increases, higher excitonic states become populated, and low-energy dark states in *H*-aggregated oligomers become observable gradually while the peak intensities near the 0−0 transition decrease for *J*-aggregated oligomers.

I. Introduction

Aggregates of π-conjugated molecules, from polymer films to crystals, have attracted enormous interest due to a wide range of applications in electronic and optoelectronic devices, such as field effect transistors (EETs)[1−3] and (organic) light emitting diodes (OLEDs).[4,5] Optical and electronic properties of the aggregates are different from those of the monomers because close intermolecular contacts in the aggregates result in strong intermolecular interactions, which are an important factor for understanding (and optimizing) device performance. Insights into these interactions can be gained by studying optical spectra of the aggregates because intermolecular interactions make their imprints on the spectra. Previous studies have revealed that photoluminescence (PL) efficiencies of *H*-aggregates and *J*-aggregates[6−9] are very different due to the different symmetry of the lowest excited state, and their PL spectra hinge on the temperature when the thermal energy is comparable to the energy spacings between their electronic states.

Recent successful synthesis of single-crystalline rubrene provides attractive application potentials due to the high hole mobility of this material, which, in the range of 10−40 cm^2/V s, is among the highest of the acenes, comparable to that of amorphous silicon.[10−12] There are many explorations focused on improving its field-effect transistor performance and investigating its transport behavior.[11−19] However, fundamental information about its intrinsic electronic structures has been still insufficient. The understanding of the effect of exposure to ambient air and visible light or oxidation on its transport characteristics and photophysical properties is also controversial. The electronic structures and photophysical properties of various materials can be investigated using photoemission measurements. Kloc and co-workers measured the PL spectra of rubrene at room temperature[20] and 20 K,[21] finding the latter blue-shifted with respect to the former. In their work, they only focused on the role of oxygen defects, while the temperature effect on the emission spectra was not systematically explained and the microscopic origins of temperature-induced behaviors remain unknown.

Additionally, unlike the rigid three-dimensional inorganic semiconductors, the conformations of the π-conjugated rubrene molecules are changed during electron transport and photoexcitation due to the strong electron−nuclear coupling. Their electronic excitation is therefore always associated with a lattice deformation. To reveal the underlying physics and understand the effects of intermolecular interactions, electron−phonon couplings, and temperature on the PL spectra of rubrene crystal, we conduct a detailed theoretical study on the vibrationally resolved absorption and emission spectra. Spectra of an isolated molecule are not difficult enough to understand. But for an aggregate, which includes a large collection of molecules, not only the intrinsic optical properties of the individual components, but also the geometrical arrangements of neighboring molecules (such as the mutual orientations and the intermolecular distances), the defects, oxidation, and the surrounding environment, can exert considerable influence on the response of a bulk sample to incident radiation. Therefore, more difficulties are encountered to understand the spectra of aggregates. The messages attained from theoretical study undoubtedly can help one to understand the spectra and reveal the effects of their own on the spectra. Additionally, spectral fitting provides us with accurate values of important structural parameters such as exciton−phonon coupling strengths and intermolecular transfer integrals, which can facilitate modeling of rubrene's physical properties.

Because of the large size of the studied systems, we combine in this work time-dependent density functional theory (TDDFT) calculations with the exciton model to theoretically investigate the absorption and PL spectra of *H*- and *J*-aggregated rubrene multichromophores. The microscopic parameters in the exciton

* To whom correspondence should be addressed. E-mail: liangwz@ustc.edu.cn (W.Z.L); yzhao@ntu.edu.sg (Y.Z.).

10.1021/jp904105p CCC: $40.75
Published on Web 10/12/2009

Hamiltonian origin from a first-principles DFT/TDDFT calculation performed on the individual chromophore or chromophore pairs.

The paper is organized as follows. Section II introduces the methodology. The vibronally resolved absorption and emission spectra of rubrene oligomers are given in section III, where we will show how the spectra evolve as the temperature fluctuates and the aggregate size increases. Detailed discussions on the microscopic origins of temperature-induced effects on PL spectra, and the spectra of mixed *H*-aggregated and *J*-aggregated rubrene multichromphores, are given in section IV. A conclusion is finally drawn.

2. The Theoretical Model

A. The Displaced Multiple Harmonic Oscillator Model. The spectral intensity related to the initial state i, weighted by the probability P_i that the initial state is occupied, can be written as

$$\begin{aligned} I(\omega) &= \sum_f \int_{-\infty}^{\infty} P_i \langle i|\mu(t)|f\rangle \cdot \langle f|\mu|i\rangle e^{-i\omega t}\, dt \\ &= \int_{-\infty}^{\infty} P_i \langle i|\mu(t)\cdot\mu|i\rangle e^{-i\omega t}\, dt \end{aligned} \tag{1}$$

Here $\mu(t) = e^{(i\hat{H}t)/\hbar}\mu e^{-(i\hat{H}t)/\hbar}$. Assuming a two-state model, within the adiabatic approximation the molecular Hamiltonian is given by

$$H = |g\rangle H_g \langle g| + |e\rangle(\omega_{eg} + H_e - i\gamma/2)\langle e| \tag{2}$$

Under the harmonic oscillator approximation, the nuclear Hamiltonians of the electronic ground and excited states for a single molecule are written, respectively, as

$$H_g^h(\mathbf{q}) = 1/2 \sum_i^n \omega_i^g [(p_i^g)^2 + (q_i^g)^2] \tag{3}$$

$$H_e^h(\mathbf{q}) = 1/2 \sum_i^n \omega_i^e [(p_i^e)^2 + (q_i^e)^2] + \omega_{eg} \tag{4}$$

Here ω_{eg} is the difference between the potential energy minima of the two electronic states with the zero-point energy correction. ω^g and ω^e denote vibrational frequencies of the electronic ground and excited states, respectively. With respect to the Hamiltonians, vibrationally resolved absorption and emission cross sections of a molecule, $\alpha(\omega)$ and $\beta(\omega)$, are calculated as

$$\alpha(\omega) \propto \omega \int_{-\infty}^{\infty} dt \exp(i\omega t - \gamma|t|)\, C_a(t) \tag{5}$$

$$\beta(\omega) \propto \omega^3 \int_{-\infty}^{\infty} dt \exp(-i\omega t - \gamma|t|)\, C_e(t) \tag{6}$$

with the dipole−dipole autocorrelation function

$$C_a(t) = \frac{\mathrm{Tr}[e^{-\beta H_g} e^{iH_g t/\hbar}\mu e^{-iH_e t/\hbar}\mu]}{\mathrm{Tr}[e^{-\beta H_g}]} \tag{7}$$

and

$$C_e(t) = \frac{\mathrm{Tr}[e^{-\beta H_e} e^{iH_e t/\hbar}\mu e^{-iH_g t/\hbar}\mu]}{\mathrm{Tr}[e^{-\beta H_e}]} \tag{8}$$

Here the dephasing factor γ is introduced to account for the influence of the environment and $\beta = 1/(KT)$. Subscripts "a" and "e" correspond to absorption and emission, respectively. The dimensionless nuclear coordinates $\mathbf{q}^g$ and $\mathbf{q}^e$ are related by

$$\mathbf{q}^e = S\mathbf{q}^g + \mathbf{D} \tag{9}$$

where $\mathbf{D}$ is the displacement between the equilibrium configurations of two electronic states and S is the Dushinsky rotation matrix which allows the ground state and the excited state to have different coordinate systems. When the momenta and positions of the nuclei change very little after photoexcitation, the intensities of vibrationally resolved electronic absorption or emission spectra can be calculated according to the Franck−Condon (FC) principle. Under the Condon approximation, the correlation function $C_{a(e)}(t)$ can be carried out analytically.[22] We have previously combined this model with TDDFT to investigate the vibrationally resolved absorption and emission spectra of conjugated polymers.[23−25] In this work the electronic absorption and emission spectra of the rubrene monomer are calculated with this model.

B. Vibrationally Coupled Frenkel Exciton Model. To calculate the spectra of aggregates with respect to the above model, one has to conduct the geometrical optimization and the vibrational frequency calculation of the ground and excited states for the aggregates. However, even low-cost TDDFT approaches are limited to small-size systems currently. Therefore, to simulate the absorption and emission spectra of aggregates, one usually uses the model Hamiltonian such as the vibrationally coupled Frenkel exciton (FE) model (see, e.g., refs 7 and 26−30). The parameters in the exciton Hamiltonian are frequently obtained by fitting the experimental spectra. Here we also utilize the exciton model, but the microscopic parameters in the model Hamiltonian are obtained from TDDFT calculations performed on an individual chromophore and a chromophore pair. Below we will give a brief description of the vibrationally coupled FE model.

The Hamiltonians of the aggregates in the weak intermolecular coupling regime can be constructed from those of the monomers. Considering an aggregate consisting of p monomers, and neglecting the weak intermolecular interactions between monomers in the electronic ground state $|g(1), g(2), ..., g(p)\rangle = |g\rangle$, one writes the ground state Hamiltonian for the aggregate with the number of p monomers as

$$H_g(q_1, ..., q_p) = |g\rangle \left[\sum_{n=1}^{p} H_g^M(q_n)\right] \langle g| \tag{10}$$

Upon excitation, p zeroth-order states are incorporated corresponding to the configurations

$$\begin{aligned} (M_1^* - M_2 - \cdots - M_p), (|e(1), g(2), \cdots, g(p)\rangle &= |e,1\rangle) \\ (M_1 - M_2^* - \cdots - M_p), (|g(1), e(2), \cdots, g(p)\rangle &= |e,2\rangle) \\ &\vdots \\ (M_1 - M_2 - \cdots - M_p^*), (|g(1), g(2), \cdots, e(p)\rangle &= |e,p\rangle) \end{aligned} \tag{11}$$

where M_n (M_n^*) denotes the nth monomer in its electronic ground (excited) state. The excited electronic configurations interact with each other via excitonic coupling J, and the excited state nuclear Hamiltonian is a $p \times p$ matrix of the form

$$H_e(q_1, \cdots, q_p) = \begin{pmatrix} H_1 & J_{12} & \cdots & J_{1,p-1} & J_{1,p} \\ J_{12} & H_2 & \cdots & J_{2,p-1} & J_{2,p} \\ & & \vdots & & \\ J_{1,p-1} & J_{2,p-1} & \cdots & H_{p-1} & J_{p-1,p} \\ J_{1,p} & J_{2,p} & \cdots & J_{p-1,p} & H_p \end{pmatrix} \quad (12)$$

with

$$H_n(q_1, \cdots, q_p) = H_e^M(q_n) - H_g^M(q_n) + \sum_{m=1}^{p} H_g^M(q_m) \quad (13)$$

In eq 12, $J_{m,n}$ is the exciton coupling between two FE states of monomers on sites m and n. Under a first-order approximation in the single excitation theory, the excitation energy-transfer coupling of two molecular fragments is approximated to be[31−33]

$$J_{m,n} = \langle \Phi_m^i | H | \Phi_n^j \rangle \quad (14)$$

Here Φ_m^i denotes the total wave function of the system with molecule m in its ith excited state Ψ_m^i and molecule n in its ground state Ψ_n^0, while Φ_n^j denotes the total wave function of the system with molecule n in its jth excited state Ψ_n^j and molecule m in its ground state Ψ_m^0. H is the Hamiltonian of the system. J is split into the following three terms as

$$J_{m,n} = J_{m,n}^{\text{coul}} + J_{m,n}^{\text{ex}} + J_{m,n}^{\text{overlap}} \quad (15)$$

where $J_{m,n}^{\text{coul}}$ and $J_{m,n}^{\text{ex}}$ are defined, respectively, as

$$\begin{aligned} J_{m,n}^{\text{coul}} &= \int d\vec{r} \int d\vec{r}\,' \, \rho_m^{i*}(\vec{r}) \frac{1}{|r - r'|} \rho_n^j(\vec{r}\,') \\ J_{m,n}^{\text{ex}} &= \int d\vec{r} \int d\vec{r}\,' \, \rho_m^{i*}(\vec{r}) g_{\text{XC}}(\vec{r}, \vec{r}\,', \omega_0) \rho_n^j(\vec{r}\,') \end{aligned} \quad (16)$$

Here $\rho_m^i(\vec{r})$ and $\rho_n^j(\vec{r}\,')$ are the transition densities of the ith excited state of molecule m at $\vec{r}$ and the jth excited state of molecule n at $\vec{r}\,'$, respectively, ω_0 is the transition frequency, and $g_{\text{XC}}(\vec{r}, \vec{r}\,', \omega_0)$ is the exchange-correlation kernel between $\vec{r}$ and $\vec{r}\,'$. For a molecular dimer, $J_{m,n}^{\text{overlap}} = -\omega_0 \int d\vec{r} \, \rho_m^{i*}(\vec{r}) \rho_n^j(\vec{r})$.

After getting the ground state and excited state Hamiltonians of aggregates, one can obtain the spectra of aggregates according to eq 5, eq 6, and eq 7. The numerical simulations are implemented in a basis set representation. The basis sets are chosen to be

$$|\phi_i\rangle = |\psi(n,k)\rangle; \quad i = (p-1) * n + k \quad (17)$$

where $|\psi(n, k)\rangle$ corresponds to the kth eigenvector ($k = 1, ..., N$) of the Hamiltonian $H_n(q_1, ..., q_p)$. In such a case, eq 12 becomes a $(p \times N) \times (p \times N)$ matrix. The Lanczos algorithm is employed to extract the low-lying eigenvalues and eigenvectors of the matrices.

In this work we assume that the electrons in a monomer (M) couple only with one effective mode ω. In this case the ground state and the excited state Hamiltonians of the monomer are simplified, respectively, into $H_g^M = -(1/2)(d^2/dq^2) + (1/2)\omega^2 q^2$, and $H_e^M = -(1/2)(d^2/dq^2) + (1/2)\omega^2(q - q_e)^2 + \Delta E_{\text{FE}}$. Then the absorption and emission spectra of the monomer are correspondingly evaluated with the following analytical formula

$$\alpha(\omega') \propto \omega' \left[\sum_{m=0} \frac{e^{-S} S^m}{m!} \Gamma(\hbar\omega' - (\Delta E_{\text{FE}} + m\omega)) \right] \quad (18)$$

$$\beta(\omega') \propto \omega'^3 \left[\sum_{m=0} \frac{e^{-S} S^m}{m!} \Gamma(\hbar\omega' - (\Delta E_{\text{FE}} - m\omega)) \right] \quad (19)$$

Here Γ is a line-shape function, and S is the Huang−Rhys factor, which is related to q_e as $S = (1/2)\omega q_e^2$. By fitting the experimental spectra or the theoretical spectra of monomer with those from the one effective oscillator model approximation, one obtains the effective frequency ω and the nuclear coordinate.

III. Results

A. The Vertical Excitation Energies of Monomer and Dimers. To understand the effect of the intermolecular interactions on the spectra and check the influence of DFT exchange-correlation (XC) functionals on electronic excitation, at first we calculate excitation energies of a rubrene monomer and three types of dimers along the a, b, and c directions. We employ both TDHF and TDDFT with the popular hybrid XC functional B3LYP[34] and the long-range-corrected (LRC) functional LRC-PBE ($\mu = 0.33/a_0$, and a_0 denotes the bohr radius).[35,36]

It has been found that TDDFT with the conventional functionals (even the popular hybrid XC functionals) provides a poor description of the polarizabilities of large extended π-conjugated systems, and the long-range intermolecular charge-transfer (CT) excitations, due to the known problems on the nonlocality and asymptotic behavior of available density functionals. Here we use the recently developed LRC-DFT scheme, LRC-PBE, to eliminate spurious CT states in TDDFT. The calculated vertical excitation energies are shown in Table 1, and the exciton couplings between the lowest Frenkel excitons are given in Table 2. A locally modified version of Q-chem[37] is employed.

In the calculations, we adopt the rubrene crystal structure as reported in ref 38. We assume that the rubrene crystal forms an orthorhombic unit cell with space group $Bbcm$ $D_{2h}^{18}(64)$ and lattice parameters $a = 7.187$ Å, $b = 14.430$ Å, and $c = 26.901$ Å. The structure of a rubrene dimer is directly extracted from the crystal in order to mimic the structural as well as spectral features of the crystalline rubrene. The molecular and crystal structures are shown in Figure 1.

As seen in Table 1, TD-B3LYP underestimates the energy of CTE for all the three types of dimers, while TDHF and TD-LRC-PBE ($\mu = 0.33/a_0$) eliminate the catastrophic underestimation of CT excitation. TD-B3LYP gives four excited states with their excitation energies lower than that of the second excited state of the monomer, which are significantly different from the results of TDHF and TD-LRC-PBE. These lowest four excited states originate from mixing the lowest intramolecular localized excitations with the lowest intermolecular CT excitations. According to the mixed Frenkel−CT exciton model, the

TABLE 1: Singlet Excitation Energies and Their Corresponding Oscillator Strengths for a Rubrene Monomer and Dimers along *a*, *b*, and *c* Directions[a]

system	states	TD-B3LYP	TDHF	TD-LRC-PBE
monomer	1	2.3333(0.1490)	2.8655(0.3782)	2.8428(0.2813)
	2	3.2791(0.0000)	3.9342(0.0001)	3.6550(0.0001)
	3		4.4881(0.0000)	4.2735(0.0000)
	4		5.3105(2.4397)	
	5		5.4578(0.0000)	
	6		5.5913(0.0982)	
dimer a	1	2.0987(0.0663)	2.8198(0.0000)	2.8131(0.0000)
	2	2.1811(0.0000)	2.8482(0.6143)	2.8376(0.4786)
	3	2.3277(0.0000)	3.9216(0.0005)	3.6450(0.0000)
	4	2.4432(0.1732)	3.9249(0.0000)	3.6454(0.0000)
	5	3.2940(0.0000)	4.4221(0.0000)	3.9695(0.0000)
	6		4.4503(0.0058)	3.9824(0.0219)
	7		4.8245(0.0000)	4.2770(0.0000)
	8		4.8797(0.0115)	4.3311(0.0003)
dimer b	1	2.2683(0.0001)	2.8328(0.0043)	2.8279(0.0044)
	2	2.2735(0.0119)	2.8893(0.6522)	2.8700(0.5129)
	3	2.3219(0.0040)	3.9319(0.0001)	3.6523(0.0002)
	4	2.3469(0.2352)	3.9346(0.0001)	3.6694(0.0001)
	5	3.2380(0.0000)	4.4821(0.0003)	4.2688(0.0000)
	6		4.5091(0.0005)	4.3023(0.0008)
	7		5.2263(0.0000)	
	8		5.2449(0.0001)	
dimer c	1	2.3234(0.3518)	2.8486(0.8738)	2.8466(0.6919)
	2	2.3404(0.0000)	2.8821(0.0000)	2.8718(0.0000)
	3	2.4319(0.0000)	3.9345(0.0000)	3.6548(0.0000)
	4	2.4320(0.0001)	3.9349(0.0001)	3.6549(0.0002)
	5	3.2789(0.0000)	4.4919(0.0000)	4.2816(0.0007)
	6		4.4997(0.0015)	4.2852(0.0007)
	7		5.2950(0.0000)	
	8		5.4859(0.0000)	

[a] The energy unit is eV.

TABLE 2: Calculated Exciton Couplings of the Three Dimers and the Energy Splittings of the Corresponding Excited States[a]

system	J	J^{coul}	$(S2 - S1)/2$	$(S4 - S3)/2$
		TD-B3LYP		
dimer a	20.87	14.78	41.2	57.75
dimer b	15.63	13.37	2.6	12.5
dimer c	−6.96	−7.80	8.5	0.05
		TDHF		
dimer a	27.86	26.66	14.20	1.65
dimer b	27.07	27.15	28.25	1.35
dimer c	−16.92	−16.94	16.75	0.2
		TD-LRC-PBE		
dimer a	22.89	23.34	12.25	0.2
dimer b	21.43	21.43	21.05	0.86
dimer c	−12.49	−12.46	12.60	0.05

[a] The energy unit is meV.

energies of CT excitons produced by TD-B3LYP are 2.192, 2.272, and 2.431 eV for dimer a, b, and c, respectively. As the CT excitons get close in energy to the lowest Frenkel excitons, both types of excitons mix effectively to form new hybrid states. The results produced by TDHF and TD-LRC-PBE ($\mu = 0.33/a_0$) also display that the stronger FE-CTE mixing takes place in dimer a, which can be corroborated by electron (hole) transfer integrals, approximately evaluated by half of energy differences of LUMO + 1 and LUMO (HOMO and HOMO − 1) as shown in Table 3.

Because the contribution from CTE to the low-lying excited states of dimers b and c is small, i.e., the through-space intercenter charge delocalization along *b* and *c* directions in

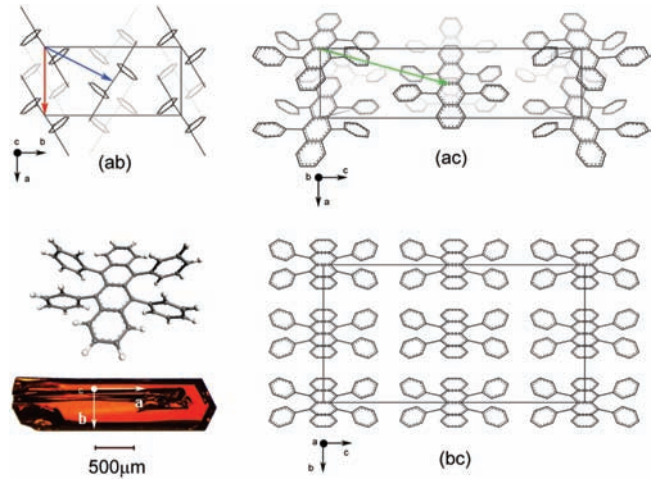

Figure 1. Molecular and crystal structure of rubrene. The *ab*, *ac*, and *bc* surfaces of the crystal are shown above, and the hydrogen atoms are omitted for clarity. Three arrows on *ab* and *ac* surfaces indicate the directions of two nearest neighbor molecules along the *a*, *b*, and *c* directions. A synthesized rubrene crystal sample is shown at the bottom left corner, where the arrows show that the largest surface is *ab*.

TABLE 3: Orbital Energies of the Three Dimers[a]

method	system	HOMO − 1	HOMO	LUMO	LUMO + 1
TD-B3LYP	dimera	−0.172	−0.164	−0.073	−0.069
	dimerb	−0.169	−0.168	−0.072	−0.072
	dimerc	−0.171	−0.171	−0.074	−0.074
TDHF	dimera	−0.224	−0.212	0.039	0.046
	dimerb	−0.220	−0.218	0.042	0.043
	dimerc	−0.221	−0.221	0.040	0.040
TD-LRC-PBE	dimera	−0.253	−0.244	−0.020	−0.014
	dimerb	−0.250	−0.249	−0.018	−0.017
	dimerc	−0.252	−0.251	−0.019	−0.019

[a] The energy unit is hartree.

rubrene crystal is insignificant, the FE model alone is efficient to simulate the spectra of oligomers b and c. However, the significant overlap between frontier orbitals on adjacent chromophores leads to through-space intercenter charge delocalization in the *a* (stacking) direction, and a mixing FE-CTE model Hamiltonian is required to correctly describe the spectra of oligomers a. Considering the large energy difference (>1 eV) between lowest FE and CTE of dimer a, one may also need to include more coupled localized FE states. Although the CT transitions usually have little intrinsic dipole strength, when they mix with FEs, the hybrid eigenstates are formed. At the end CT transitions lead to the substantial changes in dipole moment, broaden the absorption bands of multimers, and produce large Stokes shift on PL. We have employed the mixed FE-CTE model to study the spectra of *H*-aggregated perylene bisimide dyes in our recent work.[39] In this work we focus on the temperature-induced behaviors and the aggregation effect on PL of both *H*- and *J*-aggregated multimers. Only the multimers along the *b* and *c* directions are treated, and those along the *a* direction do not get involved. The FE model is employed.

B. Vibrationally Resolved Electronic Absorption and Emission Spectra of Monomer. Limited by computational resources, we perform calculations of optical spectra using the displaced multiple harmonic oscillator model for the rubrene monomer only. The equilibrium geometries, normal coordinates, and vibrational frequencies of ground and excited states of the rubrene monomer are calculated at the B3LYP/SVP and TD-B3LYP/SVP theoretical levels within the TURBOMOLE software package,[40] respectively. The SVP basis set is comparable

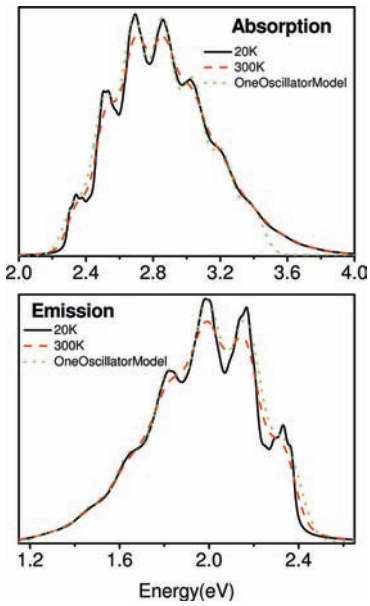

Figure 2. (Color online) Calculated absorption and emission spectra of a rubrene monomer at $T = 0$ and 300 K with the displaced multiple harmonic oscillator model. The spectra fitted with the one effective oscillator model are also included for comparison. The vertical axis is in arbitrary units.

to the popular Pople basis set 6-31G(d). In the calculation of the optical spectra, we set the dephasing factor γ to 110 cm^{-1} and the 0−0 transition energy ω_{eg} to 2.36 eV. The calculated PL spectra of rubrene monomers at 20 and 300 K are shown in Figure 2 together with the fitting spectra using the one effective harmonic oscillator model. Because of its single-mode nature, the vibrationally coupled FE model is not capable of reproducing the fine structure of each peak as well as the temperature effect on this spectral feature, which was revealed by the displaced multiple harmonic oscillator model. We only focus on the positions of the peaks and their relative intensities. As shown in Figure 2, the multimode method and its single-mode approximation agree with each other very well for both absorption and emission spectra. The fitting parameters $\omega =$ 0.175 eV, $\Delta E_{FE} = 2.3333$ eV, and $q_e = 29.50/(\sqrt{}$hartree) will be used to calculate the spectra of rubrene aggregates later.

C. Spectra of *H*- and *J*-Aggregated Oligomers. Here we consider the aggregation effect by altering the mutual orientation of the neighbor chromophores. The vibrationally coupled FE model is used to calculate the aggregate spectra.

1. H-Aggregated Oligomers. The value of the exciton coupling J is positive along the b direction, and this is indeed the case for H aggregates. We take the aggregates along this direction as an example to illustrate the temperature effect on PL of H aggregates. Here we set the exciton coupling value to be $J = 21.43$ meV which comes from the TD-LRC-PBE calculation. Due to the large value $\omega = 0.175$ eV of the effective frequency, we neglect the temperature effect on the population of ground states. The spectra of the aggregates with the different number of chromophores are shown in Figure 3.

In agreement with the Frenkel exciton theory, the absorption spectra show a slight blue shift in this case which can be easily seen in Figure 4. As the aggregate size increases, the vibrational level carrying the strongest oscillator strength converges to a higher energy, which corresponds to a blue shift. As seen from Figure 3, the emission spectra have a strong temperature dependence. The 0−0 transition is absent at low temperatures due to symmetry considerations, and it becomes appreciable as

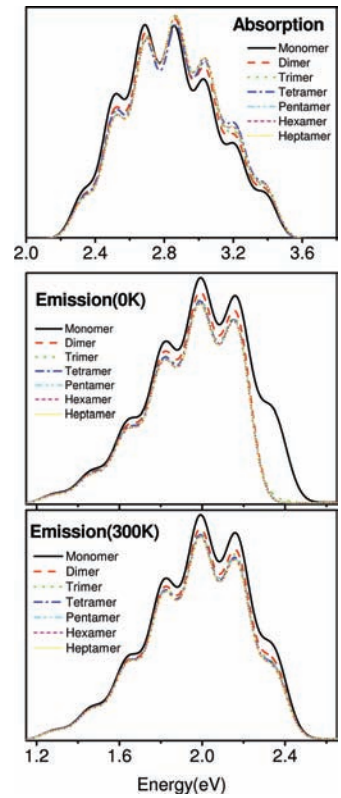

Figure 3. (Color online) Calculated absorption and emission spectra at two temperatures for oligomers along the b direction. The temperature has little effect on the absorption spectra, so only one red dashed line is shown for the absorption spectra for each oligomer. The black solid lines are the fitted spectra of the monomer. The vertical axis is in arbitrary units.

the temperature increases. This effect can be explained by the energy-level intervals and the temperature-induced alternations of populations of the vibrational states. If no coupling exists, the excited vibrational states are equally spaced by ~0.175 eV, but after accounting for the coupling J, each vibrational state expands to one phonon band as shown in Figure 4. The transition from the first phonon band to the ground state corresponds to the 0−0 transition in the spectra, and the relative thermal population distribution among the levels of the first phonon band depends very much on temperature. As for dimer b, the energy spacings of the lowest three neighbor excited states become ~0.002 620 eV and ~ 0.1676 eV. The second vibrational excited state can easily be thermally populated. The relative population distributions of the lowest two states are very much dependent on temperature. For example, at $T = 20$ K, the populations of the first two vibrational excited states are ~0.8206 and ~0.1794, while at $T = 300$ K, they become ~0.5241 and ~0.4736, respectively. Thus at lower temperatures, only the lowest vibrational level of the first phonon band which carries little oscillator strength is populated making the 0−0 transition absent in spectra, while at higher temperatures, the vibrational level which carries oscillator strength is populated making the 0−0 transition appear.

2. J-Aggregated Oligomers. The value of J is negative along the c direction, and therefore a multimer along this direction can be considered as a J aggregate. Here we take aggregates along the c direction as an example to illustrate the temperature effect on PL of J aggregates. In this case, we set the value of exciton coupling to be $J = -12.49$ meV. The spectra of aggregates is shown in Figure 5 together with the spectra of the monomer. In agreement with the Frenkel exciton theory,

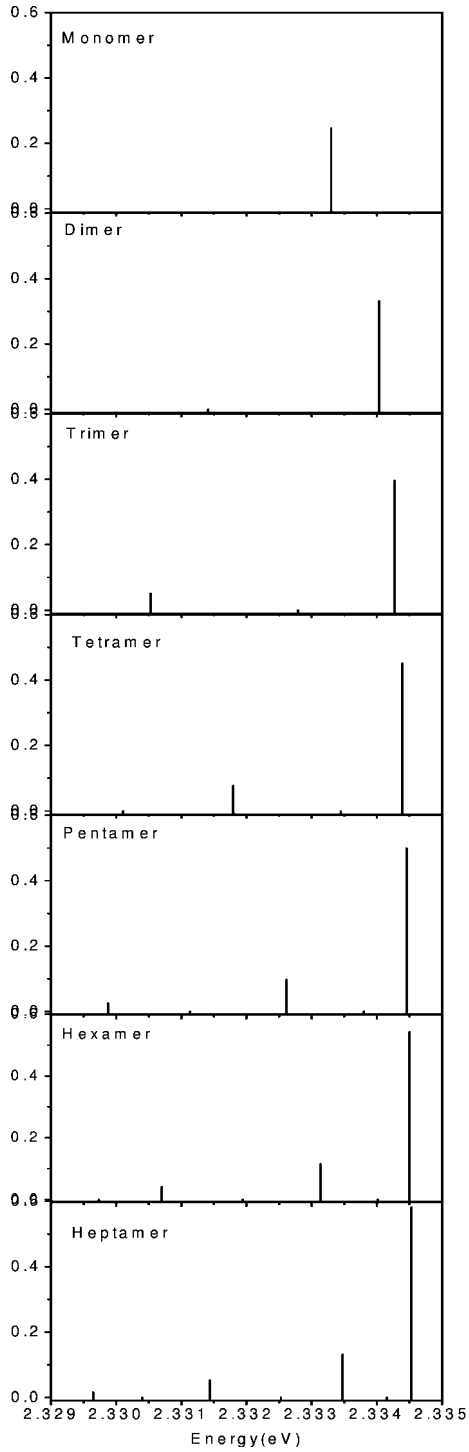

Figure 4. Calculated oscillator strength of the first phonon band of oligomers along the *b* direction; the energy of the ground state is taken as zero. The oscillator strength for the monomer is also shown for comparison.

the absorption spectra is slightly red-shifted, which can be easily seen in Figure 6. The vibrational level carrying the strongest oscillator strength converges to a lower energy as the aggregate size increases, which corresponds to a red shift.

As we can see from Figure 5, the intensity of the highest-energy emission band increases with decreasing temperature. This effect can also be explained by the oscillator strength distribution of the first phonon band. The temperature fluctuations can easily alter the relative population distribution among the levels in the first phonon band. For example, for dimer along

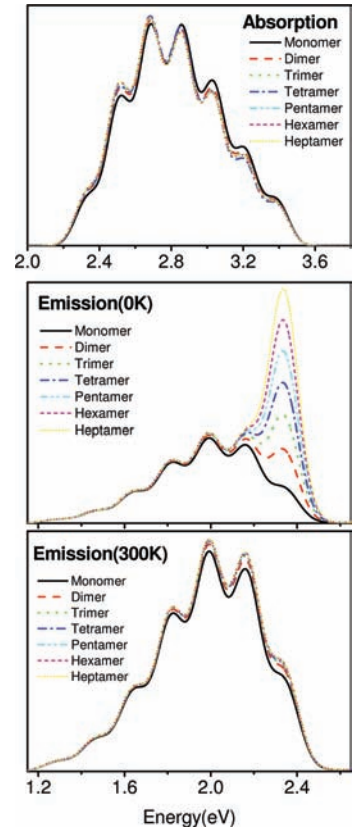

Figure 5. (Color online) Calculated absorption and emission spectra at different temperatures for oligomers along the *c* direction. The temperature has little effect on the absorption spectra, so only one red dashed line is shown for the absorption spectra for each oligomer. The black solid lines are the fitted spectra of the monomer. The vertical axis is in arbitrary units.

the *c* direction, the two energy spacings among the first three vibrational excited states are ~0.0015 and ~0.1707 eV, and at 20 K, the occupation probabilities of the first two vibrational excited states are ~0.7076 and ~0.2924, respectively, while at 300 K, the numbers become ~0.5135 and ~0.4842, respectively. At lower temperatures, only the lowest vibrational level of the first phonon band which carries the largest oscillator strength is populated making the 0−0 transition much stronger in spectra, while at higher temperatures, more electrons are populated in the higher vibrational level, which carries little oscillator strength, making the intensity of the 0−0 transition become weaker.

IV. Discussions and Concluding Remarks

To shed more light on the temperature-induced effect on the spectra, we present a detailed analysis on the coupled excitonic states which can be obtained by solving the time-independent Schrödinger equation, $H_e|\psi^i\rangle = E_i|\psi^i\rangle$. The energies of the first six excitonic states of dimer b and dimer c are give in Table 4 with "symm" and "asymm" indicating the symmetric and antisymmetric excitonic states, respectively. The wave function contours for the first six excitonic states of dimer b and dimer c are plotted in Figure 7. These states can be classified by symmetry as symmetric or antisymmetric upon reflection about a mirror plane, that is, $q_1 = q_2$ (q_1 and q_2 are two normal phonon coordinates of the dimer described by a two-dimensional harmonic oscillator). Therefore, for dimer b, the lowest excitonic state is antisymmetric and the second lowest excitonic state is symmetric, while the lowest excitonic state of dimer *c* is symmetric and the second lowest excitonic state is antisymmetric.

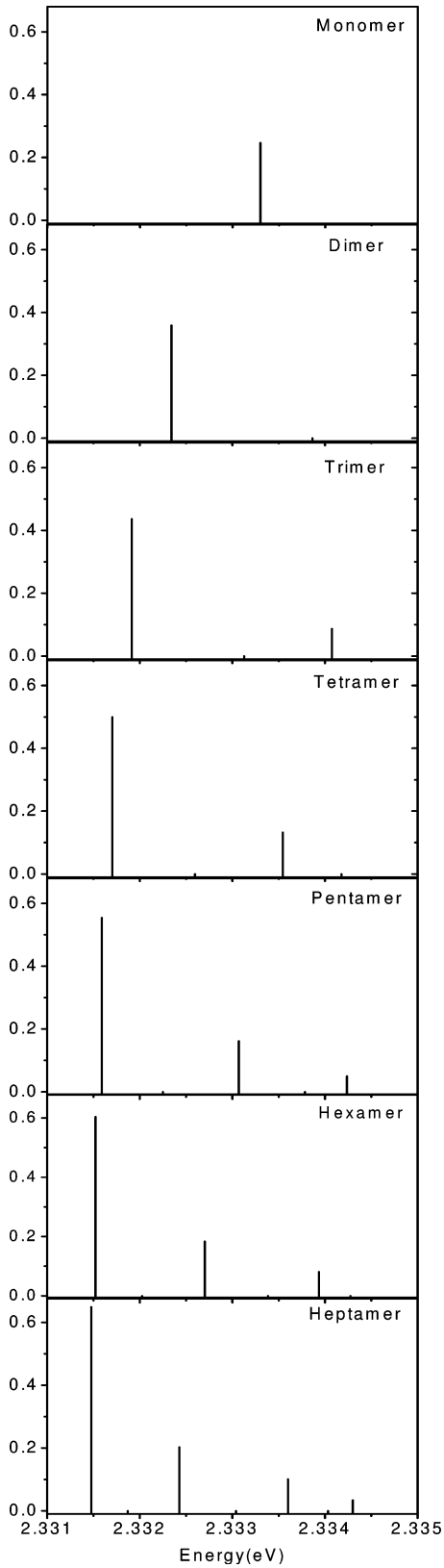

Figure 6. Calculated oscillator strength of the first phonon band of oligomers along the *c* direction; the energy of the ground state is taken as zero. The oscillator strength for the monomer is also shown for comparison.

It has been assumed that the Hamiltonian of the dimer's ground state is just that of a two-dimensional isotropic harmonic oscillator. If the total vibrational quanta of the two-dimensional harmonic oscillator are N for one vibronic state, then the degeneracy of this state is $(N + 1)$. So only the lowest level with zero vibrational quanta is nondegenerate and totally symmetric, while the other levels are degenerate containing nonsymmetric and symmetric wave functions. For example, the third lowest vibrational level of the dimer's ground state is triply degenerate, the three degenerate wave functions are (2, 0), (0, 2) and (1, 1), the former two wave functions are nonsymmetric, and the last one is symmetric.

TABLE 4: Energies of Excitonic States of Dimer b and Dimer c with Their Symmetries Being Indicated in Parentheses[a]

state	dimer b	dimer c
1	2.5064(asymm)	2.5073(symm)
2	2.5090(symm)	2.5089(asymm)
3	2.6767(asymm)	2.6796(symm)
4	2.6815(asymm)	2.6824(symm)
5	2.6841(symm)	2.6839(asymm)
6	2.6886(symm)	2.6866(asymm)

[a] The energy unit is eV.

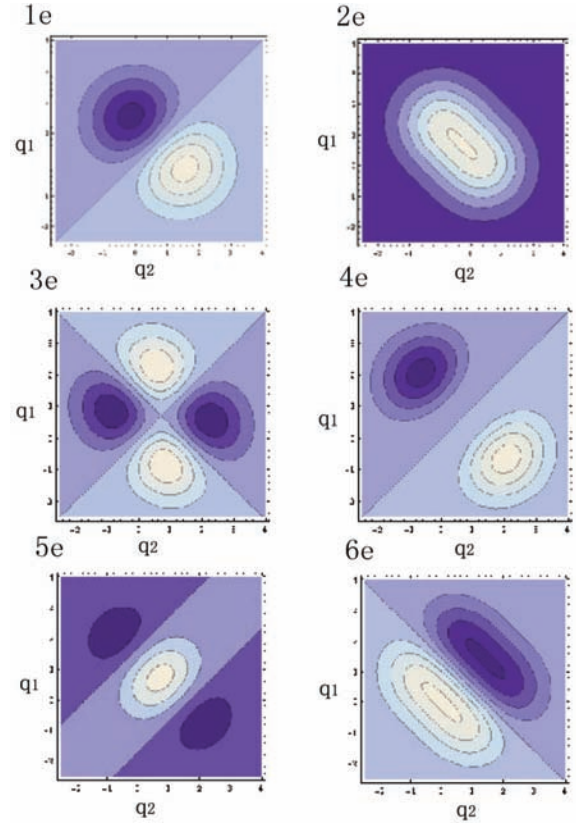

Figure 7. (Color online) Contour plots of wave functions of the first six dimer excitonic states. q_1 and q_2 are the two normal phonon coordinates. For dimer b, the first six excitonic states are 1e, 2e, 3e, 4e, 5e, and 6e, respectively, while for dimer c, the first six excitonic states are 2e, 1e, 6e, 5e, 4e, and 3e, respectively.

The ground state wave function can be written as

$$|g\rangle = |0, k_1, k_2\rangle$$

where k_1 and k_2 are the vibrational quanta of monomer 1 and monomer 2, respectively, and the excitonic state is a linear combination of Frenkel excitons

$$|e\rangle = \sum_{k_3,k_4} (C_{1,k_3,k_4}|1,k_3,k_4\rangle + C_{2,k_3,k_4}|2,k_3,k_4\rangle)$$

where, for example, $|1,k_3,k_4\rangle$, 1 means the Frenkel exciton located at monomer 1, and k_3 and k_4 are the vibrational quanta of monomer 1 and monomer 2, respectively. According to the Fermi golden rule, the intensity of the transition from $|e\rangle$ to $|g\rangle$ is proportional to the following integral

$$\begin{aligned}\langle g|\mu|e\rangle &= \langle 0,k_1,k_2|\mu| \\ &\sum_{k_3,k_4} (C_1,k_3,k_4|1,k_3,k_4\rangle + C_2,k_3,k_4|2,k_3,k_4\rangle) \\ &\sum_{k_3,k_4} (\mu_1 C_1,k_3,k_4\langle k_1|k_3\rangle_{ge}\langle k_2|k_4\rangle_{gg} \\ &+ \mu_2 C_{2,k_3,k_4}\langle k_1|k_3\rangle_{gg}\langle k_2|k_4\rangle_{ge}) \\ &= \sum_{k_3} (\mu_1 C_{1,k_3,k_2}\langle k_1|k_3\rangle_{ge} + \mu_2 C_{2,k_1,k_3}\langle k_2|k_3\rangle_{ge}\end{aligned}$$

Here $k_3 = k_4$ is assumed. μ_1 and μ_2 denote the transition dipole moments of the two monomers (for dimer we have $\mu_1 = \mu_2$), the subscript "ge" means the Franck−Condon integral of the monomer, and "gg" means the overlap integral of two vibronic wave functions (orthogonalized) of one harmonic oscillator.

If $|g\rangle = |0, n_1, n_2\rangle$ (symmetric), then

$$\langle g|\mu|e\rangle = \sum_{n_3} (\mu_1 C_{1,n_3,n_1}\langle n_1|n_3\rangle_{ge} + \mu_2 C_{2,n_1,n_3}\langle n_1|n_3\rangle_{ge})$$

For the excitonic state 1 of dimer b, we have $C_{1,n_3,n_1} = -C_{2,n_1,n_3}$, so the transition from this excitonic state to the symmetric ground state $|n_1, n_2\rangle$ is forbidden due to the phase relation between intramolecular vibrations. And if we take $|g\rangle = |n_1, n_2\rangle$ nonsymmetric, that is, $n_1 \neq n_2$, then the integral $\langle g|\mu|e\rangle$ will be nonzero and the transition will be optically observed.

To gain more insight into the effect of this symmetry classification, we calculated the emission spectra assuming that only the lowest (excitonic state 1) or the second lowest excitonic state (excitonic state 2) is populated. The results are shown in Figures 8 and 9. The peak around 2.33 eV corresponds to the transition from the corresponding excitonic state to the lowest dimer ground state. Its absence indicates the transition is symmetry forbidden, while its presence indicates the transition is symmetry allowed. As we can see, the transition from excitonic state 1 of dimer b or excitonic state 2 of dimer c to the lowest dimer ground state is symmetry forbidden, while that from excitonic state 2 of dimer b or excitonic state 1 of dimer c is symmetry allowed. The appearance of the sidebands in the spectra indicates that the transition from that excitonic state, which is assumed to be populated exclusively, to the other vibrational levels of the dimer ground state with nonsymmetric wave functions is symmetry allowed. This non-Condon emission (the sidebands of a forbidden transition are activated) is the result of the quantum interference of the Frenkel exciton states.[41,42] However, as seen in Figure 8 and Figure 9, this non-Condon emission is absent in the PL spectra of the symmetric excitonic states. Similarly, in addition to the two lowest excitonic states, the other four excitonic states can also be classified as symmetric or antisymmetric by whether the peak around 2.51 eV (corresponding to the transition from this excitonic state to the lowest dimer ground state) is present in the emission spectra assuming the corresponding excitonic state is exclusively populated.

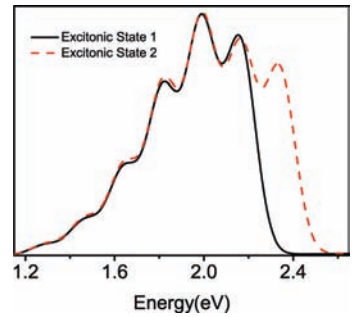

Figure 8. (Color online) Calculated emission spectra for dimer along the *b* direction assuming that excitonic state 1 or 2 is exclusively populated. Excitonic state 1 refers to the lowest excitonic state, while excitonic state 2 refers to the second lowest excitonic state. Emission intensities are given in arbitrary units.

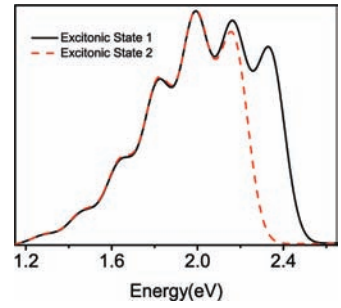

Figure 9. (Color online) Calculated emission spectra for dimer along the *c* direction assuming that excitonic state 1 or 2 is exclusively populated. Excitonic state 1 refers to the lowest excitonic state, while excitonic state 2 refers to the second lowest excitonic state. Emission intensities are given in arbitrary units.

The PL spectra at a certain temperature is just the sum of the spectra of all the excitonic states weighted by their thermal populations. So it is easy to understand the spectra of the dimers in Figure 3 and Figure 5. As mentioned in the above section, the populations of the first two lowest excitonic states dominate at temperatures lower than 300 K, and the population weight of excitonic state 2 increases with T. The PL spectra at 0 K mainly comes from electronic transition from excitonic state 1, so the 0−0 peak around 2.33 eV is absent in Figure 3 for dimer b and appreciable in Figure 5 for dimer c. When the temperature increases, the 0−0 peak intensity gradually increases for dimer b and decreases for dimer c.

As for both dimer b and dimer c, the oscillator strength in the first phonon band only has two values (one is the biggest and the other is zero) according to which we can give a definite symmetry classification of the excitonic states. When the aggregate size increases, the excitonic states do not have a definite symmetry classification as those of the dimers, and the strength has a wider distribution, which is also determined by the phase relation of the phonon modes of different chromophores. This relation can also be reflected by the intensity of the 0−0 transition in the emission spectra assuming this excitonic state is exclusively populated.

In the absorption spectra, the 0−0 line is apparently present due to the allowed transition from the ground state with $n = 0$ to the first phonon band no matter which excitonic state in the phonon band carries the strongest oscillator strength. However, at all the range of temperatures ($T = 0-300$ K), only the lowest ground state is significantly populated; therefore, the temperature effect on the absorption spectra is not appreciable.

In order to account for both *H*- and *J*-type couplings in the crystal, Figure 11 displays the spectra for a rubrene tetramer

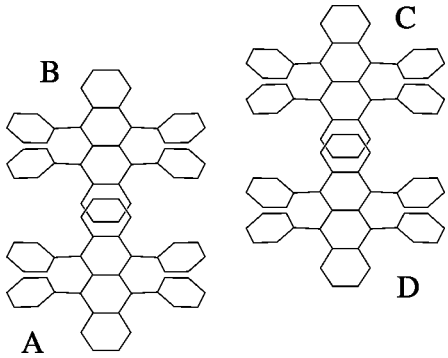

Figure 10. Tetramer configuration used in the work. Parameters adopted in the calculation: $J_{AB} = J_{CD} = 21.43$ meV, $J_{AD} = J_{BC} = J_{BD} = -12.49$ meV. J_{AC} is set to zero.

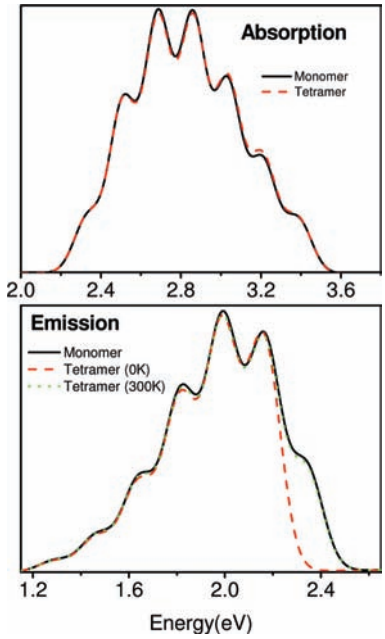

Figure 11. (Color online) Calculated absorption and emission spectra for a tetramer shown in Figure 10. There is little temperature effect on the absorption spectra, so only one line is shown for the absorption spectra in the upper panel. The vertical axis is in arbitrary units.

shown in Figure 10. As we can see, the temperature-dependent behavior is similar to those of *H* aggregates. This is easily explained by the fact that the magnitude of *H*-type coupling in the tetramer is twice as large as that of *J*-type coupling. Figure 12 plots the oscillator strength distribution. The fact that the lowest excitonic state in the first phonon band carries little oscillator strength induces the same phenomenon as *H*-type aggregates shown in the above section. We may expect that the optical emission of rubrene thin film is dominated by the coupled *H* aggregates.

Spano and co-workers[43] have studied aggregate emission in regioregular polythiophene and concluded that optical emission is overwhelmingly dominated by weakly coupled *H* aggregates. Their temperature-dependent PL spectra show a systematic increase of the 0−0 peak intensity with temperature, which qualitatively agrees with our conclusion about *H*-type aggregate here. The dynamic red shift and the loss of 0−0 peak intensity with time in the time-resolved PL spectra at 10 K just indicate energy diffusion to more ordered domains.

As for *J*-type coupling, the intensity of the 0−0 peak should increase with decreasing temperature. The attenuation of the 0−0 transition at lower temperature can be called subradiance,

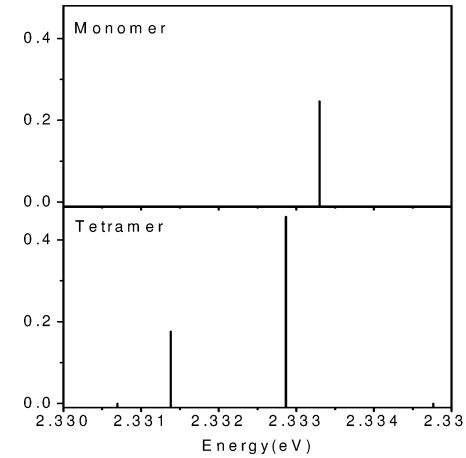

Figure 12. Calculated oscillator strength of the first phonon bands of the tetramer shown in Figure 10; the energy of the ground state is taken as zero. The oscillator strength for the monomer is also shown for comparison.

which is also the result of coherent emission. The excitonic coherence is lost (dephasing) as the temperature increases, which thus induces the destruction of superradiance or subradiance. The influence of temperature on supperradiance (subradiance) discussed here coincides with the conclusions by Zhao and co-workers.[44] Energetic disorder is another factor which affects the exciton coherence.[44,50−54] In addition to temperature and disorder-induced dephasing, polaronic effects can also destroy excitonic coherence and take control of the superradiance (subradiance).[44−46] For example, self-trapping will occur when the Huang−Rhys factor is large[47−49] for weakly coupled aggregates. The polaronic effects, which may be important for the rubrene single crystal, are overlooked by our model as our exciton wave function is not distorted by phonon.

To conclude, spectra simulation of the aggregates shows that *H*-aggregated coupling and *J*-aggregated coupling will induce distinctly different temperature-dependent behavior on PL spectra which can be explained by the exciton−phonon coupling. This temperature-induced behavior can give us some hints toward understanding the experimentally observed temperature-dependent spectral characteristics of aggregates.

Our current work is mainly focused on the temperature-induced behavior and the aggregation effect on PL spectra of both *H*- and *J*-aggregated rubrene multimers. Only the multimers along *b* and *c* directions in rubrene crystal are taken into account. Therefore our calculated spectra should be different from those of rubrene crystal. The multimers along the *a* direction should play the dominate role in the spectral characteristics of rubrene crystal. Further work which includes the chromophores in all the directions, and considers the contributions from CTEs, is essential to produce the experimental spectra of rubrene crystal. We expect to report the results in the near future.

Acknowledgment. Financial support from National Science Foundation of China (Nos. 20673104, 20833003), a 973 project funded by National Basic Research Program of China (Nos. 2004CB719901 and 2006CB922004), and Chinese Academy of Science are acknowledged.

Note Added after ASAP Publication. This article was published on October 12, 2009. Reference 2 was revised and the corrected version was reposted on October 28, 2009.

References and Notes

(1) Horowitz, G. *Adv. Mater.* **1998**, *10*, 365.

(2) Zeis, R.; Besnard, C.; Siegrist, T.; Schlockermann, C.; Chi, X.; Kloc, C. *Chem. Mater.* **2006**, *18*, 244–248.
(3) Meijer, E. J.; Deleeuw, D. M.; Setayesh, S.; Van Veenendaal, E.; Huisman, B.-H.; Blom, P. W. M.; Hummelen, J. C.; Scherf, U.; Klapwijk, T. M. *Nat. Mater.* **2003**, *2*, 678.
(4) Chen, C.-T. *Chem. Mater.* **2004**, *16*, 4389.
(5) Tessler, N.; Medvedev, V.; Kazes, M.; Kan, S. H.; Banin, U. *Science* **2002**, *295*, 1506.
(6) Mukamel, S.; Abramavicius, D. *Chem. Rev.* **2004**, *104*, 2073.
(7) Spano, F. C. *Annu. Rev. Phys. Chem.* **2006**, *57*, 217.
(8) Bredas, J.-L.; Beljonne, D.; Coropceanu, V.; Cornil, J. *Chem. Rev.* **2004**, *104*, 4971.
(9) May, V.; Kühn, O. *Charge and Energy Transfer Dynamics in Molecular Systems*; Wiley-VCH: New York, 2005.
(10) Takeya, J.; Yamagishi, M.; Tominari, Y.; Hirahara, R.; Nakazawa, Y.; Nishikawa, T.; Kawase, T.; Shimoda, T.; Ogawa, S. *Appl. Phys. Lett.* **2007**, *90*, 102120.
(11) Podzorov, V.; Menard, E.; Borissov, A.; Kiryukhin, V.; Rogers, J. A.; Gershenson, M. E. *Phys. Rev. Lett.* **2004**, *93*, 086602.
(12) Hulea, I. N.; Fratini, S.; Xie, H.; Mulder, C. L.; Iossad, N. N.; Rastelli, G.; Ciuchi, S.; Morpurgo, A. F. *Nat. Mater.* **2006**, *5*, 982.
(13) Sundar, V. C.; Zaumseil, J.; Podzorov, V.; Menard, E.; Willett, R. L.; Someya, T.; Gershenson, M. E.; Rogers, J. A. *Science* **2004**, *303*, 1644.
(14) Ostroverkhova, O.; Cooke, D. G.; Hegmann, F. A.; Anthony, J. E.; Podzorov, V.; Palstra, T. T. M. *Appl. Phys. Lett.* **2006**, *88*, 162101.
(15) Podzorov, V.; Pudalov, V. M.; Gershenson, M. E. *Appl. Phys. Lett.* **2004**, *85*, 6039.
(16) Takahashi, T.; Takenobu, T.; Takeya, J.; Iwasa, Y. *Appl. Phys. Lett.* **2006**, *88*, 033505.
(17) Krellner, C.; Haas, S.; Goldmann, C.; Pernstich, K. P.; Gundlach, D. J.; Batlogg, B. *Phys. Rev. B* **2007**, *75*, 245115.
(18) Li, Z. Q.; Podzorov, V.; Sai, N.; Martin, M. C.; Gershenson, M. E.; Ventra, M. D.; Basov, D. N. *Phys. Rev. Lett.* **2007**, *99*, 016403.
(19) So, W.-Y.; Wikberg, J. M.; Lang, D. V.; Mitrofanov, O.; Kloc, C. L. *Solid State Commun.* **2007**, *142*, 483.
(20) Mitrofanov, O.; Kloc, C.; Siegrist, T.; Lang, D. V.; So, W.-Y.; Ramirez, A. P. *Appl. Phys. Lett.* **2007**, *91*, 212106.
(21) Mitrofanov, O.; Lang, D. V.; Kloc, C.; Wikberg, J. M.; Siegrist, T.; So, W.-Y.; Sergent, M. A.; Ramirez, A. P. *Phys. Rev. Lett.* **2006**, *97*, 166601.
(22) Yan, Y. J.; Mukamel, S. *J. Chem. Phys.* **1986**, *85*, 5908.
(23) Liang, W. Z.; Zhao, Y.; Sun, J.; Song, J.; Hu, S. L.; Yang, J. L. *J. Phys. Chem. B* **2006**, *110*, 9908.
(24) Song, J.; Liang, W. Z.; Zhao, Y.; Yang, J. L. *Appl. Phys. Lett.* **2006**, *89*, 071917.
(25) Gao, F.; Zhao, Y.; Liang, W. Z. *J. Chem. Phys.* **2007**, *126*, 224509.
(26) Renger, T.; Voigt, J.; May, V.; Kühn, O. *J. Phys. Chem.* **1996**, *100*, 15654.
(27) Seibt, J.; Dehm, V.; Würthner, F.; Engel, V. *J. Chem. Phys.* **2007**, *126*, 164308.
(28) Seibt, J.; Engel, V. *Chem. Phys.* **2008**, *347*, 120.
(29) Seibt, J.; Marquetand, P.; Engel, V.; Chen, Z.; Dehm, V.; Würthner, F. *Chem. Phys.* **2006**, *328*, 354.
(30) Fink, R. F.; Seibt, J.; Engel, V.; Renz, M.; Kaupp, M.; Lochbrunner, S.; Zhao, H.-M.; Pfister, J.; Würthner, F.; Engels, B. *J. Am. Chem. Soc.* **2008**, *130*, 12858.
(31) McWeeny, R. *Methods of Molecular Quantum Mechanics*, 2nd ed.; Academic Press: London, U.K., 1992.
(32) Hsu, C.-P.; Fleming, G. R.; Head-Gordon, M.; Head-Gordon, T. *J. Chem. Phys.* **2001**, *114*, 3065.
(33) Scholes, G. D. *Annu. Rev. Phys. Chem.* **2003**, *54*, 57.
(34) Becke, A. D. *J. Chem. Phys.* **1993**, *98*, 5648.
(35) Vydrov, O. A.; Scuseria, G. E. *J. Chem. Phys.* **2006**, *125*, 234109.
(36) Song, J.-W.; Hirosawa, T.; Tsuneda, T.; Hirao, K. *J. Chem. Phys.* **2007**, *126*, 154105.
(37) Shao, Y.; Fusti-Molnar, L.; Jung, Y.; Kussmann, J.; Ochsenfeld, C.; Brown, S. T.; Gilbert, A. T. B.; Slipchenko, L. V.; Levchenko, S. V.; ONeill, D. P.; Distasio, R. A., Jr.; Lochan, R. C.; Wang, T.; Beran, G. J. O.; Besley, N. A.; Herbert, J. M.; Lin, C. Y.; Van Voorhis, T.; Chien, S. H.; Sodt, A.; Steele, R. P.; Rassolov, V. A.; Maslen, P. E.; Korambath, P. P.; Adamson, R. D.; Austin, B.; Baker, J.; Byrd, E. F. C.; Dachsel, H.; Doerksen, R. J.; Dreuw, A.; Dunietz, B. D.; Dutoi, A. D.; Furlani, T. R.; Gwaltney, S. R.; Heyden, A.; Hirata, S.; Hsu, C.-P.; Kedziora, G.; Khalliulin, R. Z.; Klunzinger, P.; Lee, A. M.; Lee, M. S.; Liang, W. Z.; Lotan, I.; Nair, N.; Peters, B.; Proynov, E. I.; Pieniazek, P. A.; Rhee, Y. M.; Ritchie, J.; Rosta, E.; Sherrill, C. D.; Simmonett, A. C.; Subotnik, J. E.; Woodcock, H. L., III; Zhang, W.; Bell, A. T.; Chakraborty, A. K.; Chipman, D. M.; Keil, F. J.; Warshel, A.; Hehre, W. J.; Schaefer, H. F., III; Kong, J.; Krylov, A. I.; Gill, P. M. W.; Head-Gordon, M. *Phys. Chem. Chem. Phys.* **2006**, *8*, 3172.
(38) Jurchescu, O. D.; Meetsma, A.; Palstra, T. T. M. *Acta Crystallogr. B* **2006**, *62*, 330.
(39) Pan, F.; Gao, F.; Liang, W. Z.; Zhao, Y. *J. Phys. Chem. B*, in press.
(40) Ahlrichs, R.; Bär, M.; Baron, H.-P.; Bauernschmitt, R.; Böcker, S.; Deglmann, P.; Ehrig, M.; Eichkorn, K.; Elliott, S.; Furche, F.; Haase, F.; Häser, M.; Horn, H.; Hättig, C.; Huber, C.; Huniar, U.; Kattannek, M.; Andreas Köhn, A.; Kölmel, C.; Kollwitz, M.; May, K.; Ochsenfeld, C.; Ohm, H.; Patzelt, H.; Rubner, O.; Schafer, S.; Schneider, U.; Sierka, M.; Treutler, O.; Unterreiner, B.; von Arnim, M.; Weigend, F.; Weis, P.; Weiss, H. *TURBOMOLE*, Ver5.6; Quantum Chemistry Group: Universität Karlsruhe, 2003.
(41) Bittner, E. R.; Karabunarliev, S.; Herz, L. M. *J. Chem. Phys.* **2007**, *126*, 191102.
(42) Banerjee, K.; Gangopadhyay, G. *J. Chem. Phys.* **2009**, *130*, 084705.
(43) Clark, J.; Silva, C.; Friend, R. H.; Spano, F. C. *Phys. Rev. Lett.* **2007**, *98*, 206406.
(44) Zhao, Y.; Meier, T.; Zhang, W. M.; Chernyak, V.; Mukamel, S. *J. Phys. Chem. B* **1999**, *103*, 3954. Meier, T.; Zhao, Y.; Chernyak, V.; Mukamel, S. *J. Chem. Phys.* **1997**, *107*, 3876.
(45) Spano, F. C.; Kuklinski, J. R.; Mukamel, S. *Phys. Rev. Lett.* **1990**, *65*, 211.
(46) Spano, F. C.; Kuklinski, J. R.; Mukamel, S. *J. Chem. Phys.* **1991**, *94*, 7534.
(47) Zhao, Y.; Brown, D. W.; Lindenberg, K. *J. Chem. Phys.* **1997**, *106*, 5622.
(48) Zhao, Y.; Brown, D. W.; Lindenberg, K. *J. Chem. Phys.* **1997**, *107*, 3159.
(49) Brown, D. W.; Lindenberg, K.; Zhao, Y. *J. Chem. Phys.* **1997**, *107*, 3179.
(50) Spano, F. C.; Meskers, S. C. J.; Hennebicq, E.; Beljonne, D. *J. Am. Chem. Soc.* **2007**, *129*, 7044.
(51) Spano, F. C. *J. Chem. Phys.* **2001**, *116*, 5877.
(52) Spano, F. C. *J. Chem. Phys.* **2005**, *122*, 234701.
(53) Spano, F. C.; Meskers, S. C. J.; Hennebicq, E.; Beljonne, D. *J. Chem. Phys.* **2008**, *129*, 024704.
(54) Spano, F. C.; Clark, J.; Silva, C.; Friend, R. H. *J. Chem. Phys.* **2009**, *130*, 074904.

JP904105P